

Single-material-substrated triboelectric–electromagnetic hybrid generator for self-powered multifunctional sensing in intelligent greenhouse

Baosen Zhang^{1,2}, Wenbo Li^{1,2}, Jianwei Ge¹, Chenggen Chen¹, Xin Yu¹, Zhong Lin Wang^{1,2,3} (✉), and Tinghai Cheng^{1,2} (✉)

¹ Beijing Institute of Nanoenergy and Nanosystems, Chinese Academy of Sciences, Beijing 101400, China

² School of Nanoscience and Technology, University of Chinese Academy of Sciences, Beijing 100049, China

³ School of Materials Science and Engineering, Georgia Institute of Technology, Atlanta, Georgia, 30332-0245, USA

© Tsinghua University Press 2022

Received: 1 July 2022 / Revised: 1 August 2022 / Accepted: 15 August 2022

ABSTRACT

The environmental micro-energy harvested by the triboelectric–electromagnetic hybrid generator (TEHG) can power sensors and Internet of Things (IoT) nodes in smart agriculture. However, the separation structure of traditional TEHG raises the complexity of form and material, which is harmful to the miniaturization of the device. Herein, a single-material-substrated triboelectric–electromagnetic hybrid generator (SMS-TEHG) based on the flexible magnets is designed to achieve the structural integration of triboelectric nanogenerator (TENG) and electromagnetic generator (EMG). The flexible magnets serve as the electropositive triboelectric materials for TENG and the magnetic materials for EMG, simplifying the structural complexity of TEHG. The open-circuit voltage (V_{OC}) of the TENG and EMG are 187.2 and 9.0 V at 300 rpm, respectively. After 30,000 cycles of stability testing, the V_{OC} of the TENG and EMG retain about 95.6% and 99.3%, respectively. Additionally, the self-powered applications driven by SMS-TEHG in intelligent greenhouse have been successfully demonstrated, such as crop light supplementation, rain monitoring, and wireless temperature and humidity sensing. This work provides a new design for TEHG and possibilities for applying TEHG and IoT in smart agriculture.

KEYWORDS

triboelectric–electromagnetic hybrid generator, single-material-substrated, wind energy harvesting, self-powered, smart agriculture

1 Introduction

The Internet of Things (IoT) and big data are widely used in smart agriculture to improve production efficiency [1–3]. The power supply of sensors in smart agriculture currently mainly relies on batteries, which need to be replaced regularly and cause environmental pollution [4, 5]. Massive numbers of sensors require new distributed power supplies to operate for extended periods of time and reduce pollution [6, 7]. Wind energy as renewable energy widely exists in agricultural environment. Considering the low power consumption of individual sensors in sensor networks, it has great potential to solve the problem of distributed power supply by converting local wind energy into electric power. Therefore, wind energy harvesters with a simple structure need to be developed to satisfy the distributed and low-power energy demand of smart agriculture.

Triboelectric nanogenerator (TENG) is an energy harvester based on the coupling effect of contact electrification and electrostatic induction invented by Wang's group in 2012 [8–13]. Due to the advantages of low cost, lightweight, and high efficiency [14–17], TENGs have been used to convert mechanical energy into electric power in various environments to supply low-power devices such as thermometers and watches [18–20]. However, the

high-frequency output performance of TENG is insufficient, and the harvested energy cannot meet the power consumption in smart agriculture. TENG can be used in cooperation with other energy harvesters, such as solar cells [21–23], electromagnetic generators (EMG) [24–26], piezoelectric nanogenerators [27, 28], and thermoelectric generators, to increase the total energy output [29–31]. Among them, the triboelectric–electromagnetic hybrid generator (TEHG) combined with TENG and EMG is commonly used to collect mechanical energy in the environment, such as wind energy [32] and vibration energy [33]. To meet the design requirements of TEHG, it is usually required to design two independent components of TENG and EMG, which leads to the disadvantage of complex mechanical structure [34–36]. Therefore, a design of simplifying the TEHG structure is needed to improve the collection of mechanical energy to provide stable green energy for sensors in smart agriculture and IoT.

Here, a single-material-substrated triboelectric–electromagnetic hybrid generator (SMS-TEHG) based on flexible magnets is proposed to collect wind energy. Different from the past design method of using different materials for the TENG part and the EMG part in the TEHG, the flexible magnet is used as the friction material of the TENG to replace the commonly used

Address correspondence to Zhong Lin Wang, zhong.wang@mse.gatech.edu; Tinghai Cheng, chengtinghai@binn.cas.cn

electropositive triboelectric materials and the magnetic material of the EMG. The combination of TENG and EMG is realized by using flexible magnets. The TENG part and the EMG part will not affect each other when operating simultaneously, which means that SMS-TEHG has the advantage of simple structure to operate stably in smart agriculture. Moreover, self-powered applications are successfully demonstrated in intelligent greenhouses powered by SMS-TEHG, including real-time rain monitoring, nighttime crop light supplementation, and wireless temperature and humidity sensing, demonstrating the potential applications of SMS-TEHG in smart agriculture.

2 Results and discussion

2.1 Structural design and operation principle

Smart agriculture relies on sensors and wireless sensing devices. At the same time, there are many wastes of natural wind energy around the agricultural production environment. The capture of natural wind energy in agricultural production is an effective supplement and alternative to the traditional power supply mode. As shown in Fig. 1(a), a single-material-substrated triboelectric–electromagnetic hybrid generator (SMS-TEHG) is developed and installed around greenhouses and farmland to collect wind energy in agricultural environment. Figure 1(b) presents the entire structure of the SMS-TEHG, which is constituted of one TENG and one EMG for power generation. The external whole of the generator is cylindrical, and the shaft extended by the internal rotor can connect various wind energy collection devices. Here, the wind spoon is taken as an example. The internal structure and the supporting structure of SMS-TEHG are composed of a stator and a rotor. The grating copper electrode with a distance of 4 mm is fixed on the cylindrical base as the electrode of TENG, and a layer of polytetrafluoroethylene (PTFE)

film adheres to the surface of the electrode as the electronegative friction material. The cylindrical base and the outer cylinder are fixed by using double-sided tape. Four flexible magnets are fixed on the rotor as electropositive triboelectric materials, forming the TENG part of SMS-TEHG. The relative motion of PTFE and flexible magnets leads to the generation of alternating current (AC) signals. The outer cylinder is designed with grooves for fixing the coil, and the four coils are uniformly fixed under the grating electrode. The coil on the stator combines the flexible magnet group on the rotor to form the EMG part of SMS-TEHG. Figure S1 in the Electronic Supplementary Material (ESM) illustrates the fabrication flow diagram of SMS-TEHG. The SMS-TEHG assembled photo is indicated in Fig. 1(c). The shell is fabricated by a three-dimensional (3D) printer, supporting the structure, isolating the external environment, and serving as the stator of SMS-TEHG. The coils are first wound by a winding machine. The arc mold is used to shape the coils to have the same arc as the stator to match the arc stator. Figure 1(d)(i) is a photo of the electrode portion of TENG, and Fig. 1(d)(ii) exhibits the coil group fixed under the electrodes. The four flexible magnets are uniformly distributed and settled on the rotor (Fig. 1(d)(iii)). Figure 1(d)(iv) illustrates that flexible magnets have better flexibility than rigid magnets.

2.2 Operational principle and simulation

The four typical phases in the working mechanism of SMS-TEHG are depicted in Fig. 2(a). Positive electrostatic charge is generated on the flexible magnet, whereas negative charge is generated on the PTFE film surface during contact electrification. The total electric charge of the flexible magnet portion and PTFE is identical due to the conservation of electric charge. With the relative rotation of the flexible magnets and the electrodes, the free charge on the electrodes will be redistributed between the two sets of electrodes by an external load to balance the change in potential

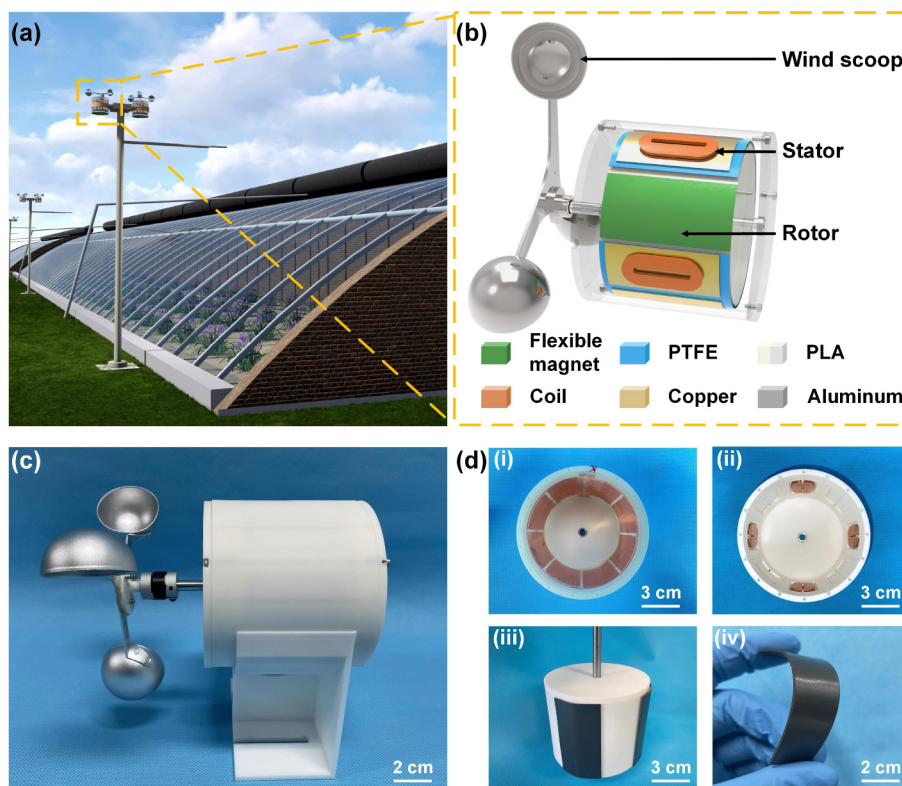


Figure 1 Mechanism design of SMS-TEHG. (a) SMS-TEHG devices are installed at intervals around the greenhouse. (b) The structural profile of SMS-TEHG exhibits that each component is coaxial. (c) Photo of the prototype. The wind scoop is installed after assembly. (d) (i) TENG unit in SM-TEHG. (ii) EMG unit in SM-TEHG. (iii) The rotor with flexible magnets is installed. (iv) The photograph of a flexible magnet unit demonstrates its flexibility.

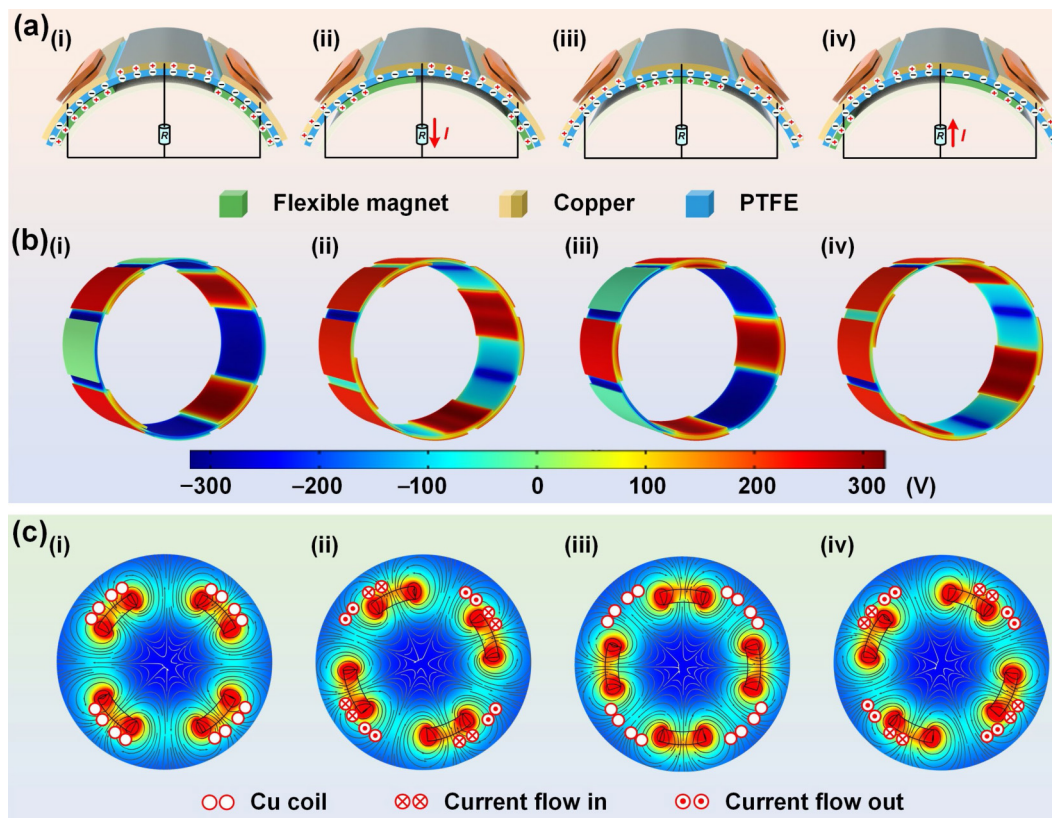


Figure 2 SMS-TEHG working mechanism. (a) The working principle of TENG in four different states. (b) The space electric fields of the four working states of TENG are simulated by COMSOL. (c) The working principle of EMG.

difference, according to the principle of electrostatic induction. Due to the existence of the periodic structure, the induced periodic charge transfer between the two sets of electrodes will produce alternating current (AC) signals. COMSOL (COMSOL Multiphysics 5.6) was used to model the electrostatic field, demonstrating the power generating mechanism of TENG (Fig. 2(b)). The EMG portion works on the basis of electromagnetic induction, which creates periodic AC signals when the magnetic flux changes (Fig. 2(c)). In the initial state, such as step (i), the magnet faces the coil, and there is no induced current. The magnetic flux in the coil drops as the magnet revolves around the axis, causing an induced current in the circular copper coil (step (ii)). As the magnets move away from the coils, the current continues to flow until the magnets and coils are completely staggered (step (iii)). Subsequently, as the magnet approaches the coil, the magnetic flux in the coil increases, causing a reverse induced current (step (iv)). The EMG signal creates a continuous alternating current due to the rotating movement. The magnetic field of the ring magnet array is analyzed, and the magnetic field exhibits periodic fluctuations on the running trajectory of the coil (Fig. S2 in the ESM).

2.3 Optimized parameters and output characteristics

The SMS-TEHG is placed in a wind tunnel, and the rotation speed of the rotor of the SMS-TEHG is recorded under different wind speeds. As illustrated in Fig. 3(a), the rotating speed is almost proportional to the wind speed. The output performance of the SMS-TEHG was tested using a servomotor as a power source in the following tests. To study the influence of the length of flexible magnet on the performance of TENG, the servo motor was used to drive SMS-TEHG at 200 rpm. As shown in Fig. 3(b), the open-circuit voltage (V_{OC}) of the flexible magnet with a length of 60–80 mm is measured by an electrometer. The results illustrate that the V_{OC} increases with the length of the flexible magnet. When the length of the flexible magnet increases from 60 to 80 mm, the V_{OC}

increases from 118.2 to 182.1 V. Simultaneously, the short-circuit current (I_{SC}) of TENG increases from 3.3 to 6.1 μA with the rise in the length of the flexible magnet (Fig. 3(c)). The voltage increase is attributed to the increase of the area corresponding to the flexible magnet and PTFE and the current increases with the increase of the voltage. When the length of the flexible magnet is 80 mm, the electric output performance of TENG is tested at 50–300 rpm. With the increase in rotating speed, the V_{OC} of TENG remains 187.2 ± 5 V, it does not change with the change of rotational speed (Fig. 3(d)) due to the constant contact area, and the I_{SC} increases from 1.0 to 7.0 μA with the increase of rotational speed (Fig. 3(e)). The performance of TENG charging to the capacitor is tested (Fig. S3 in the ESM). As shown in Fig. 3(f), to demonstrate the output performance of TENG under different external loads, at the speed of 200 rpm, the resistor box was used to connect different resistors on the output electrode of TENG as the load. When the resistor increases, the voltage increases from 0.2 to 179.3 V; the current decreases from 6.6 to 0.7 μA , and the output power first increases to a peak of 0.8 mW at 30 M Ω and then decreases. The output performance of TENG is tested at different rotating speeds with the load of 30 M Ω . (Fig. S4 in the ESM). It is a common strategy for TENG to charge the capacitor first and then power the appliance. The stability of TENG was tested, and its V_{OC} retains about 95.6% after the 30,000 cycles, which maintains good stability (Fig. 3(g)). The surface of the flexible magnet has no noticeable change before and after the stability test under the light microscope (Fig. 3(h)), which may be the reason for maintaining the stability of the performance. Relative humidity, as an essential changing factor in agricultural production, will have a particular impact on the performance of TENG. At 25 $^{\circ}\text{C}$, the performance of TENG was tested at different relative humidity (200 rpm). When the relative humidity is 90%, the I_{SC} is reduced by 13% compared with 30% (Fig. 3(i)), which may be attributed to the shell of the SMS-TEHG that isolates the power generation unit from the external environment.

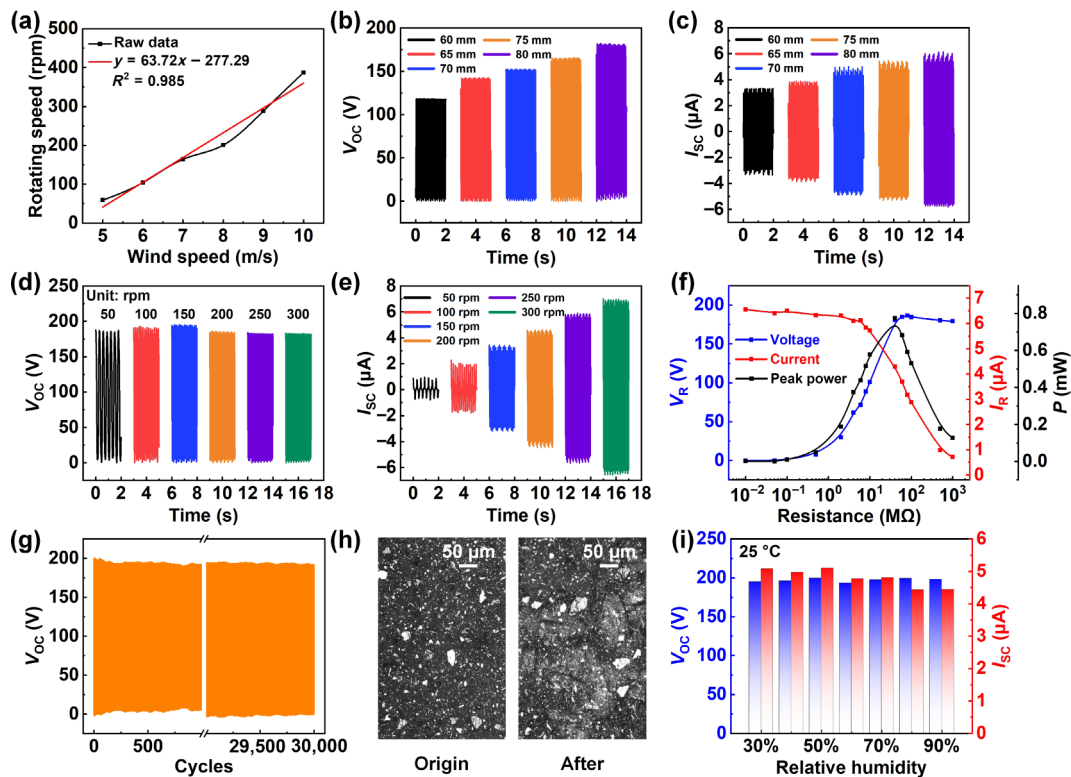


Figure 3 Performance test of TENG part. (a) The wind speed corresponds to the speed of the servomotor. (b) V_{OC} and (c) I_{SC} of different magnet lengths. (d) V_{OC} and (e) I_{SC} of the electrode at different rotating speeds. (f) Output performance with different loads under a rotating speed of 200 rpm. (g) TENG stability test at 50 rpm. (h) Surface morphology of flexible magnets before and after stability test. (i) TENG output test at different relative humidity.

In previous studies, TEHGs generally consisted of two separate parts, which resulted in complex structures and late maintenance. In SMS-TEHG, the EMG coil group is fixed on the back of the electrode, and there is a TENG electrode barrier between the coil and the magnet. As shown in Fig. 4(a) and Fig. S5 in the ESM, there is no difference in the output performance of the EMG between the coil and the flexible magnet with and without TENG at 200 rpm. The number of coils affects the output performance of EMG. When the speed is 200 rpm, the output performance of EMG is tested by changing the number of coils. For EMG, V_{OC} can be expressed as

$$V_{OC} = n \frac{d\phi}{dt} \quad (1)$$

Among them, n is the total number of turns, and the change of the magnetic flux with time is $\frac{d\phi}{dt}$. The V_{OC} increases linearly with the increase in the number of coils (Fig. 4(b) and Eq. (1)).

$$I_{SC} = \frac{V_{OC}}{R_0} = \frac{n \frac{d\phi}{dt}}{nR_1} = \frac{d\phi}{R_1 dt} \quad (2)$$

where I_{SC} is the short circuit current of the EMG; R_0 is the total resistance of the coil; R_1 is the resistance of a single turn. The I_{SC} does not change with the number of coils because the internal resistance of the EMG rises with the number of coils (Fig. 4(c) and Eq. (2)). This is because the coils are connected in series. When the numbers of coils and magnets are same, the force of the shaft in each direction is equal, which is beneficial to reducing wear. Four coils were used in the following tests to obtain higher output performance. In order to study the effect of rotational speed on the performance of EMG, the electric signal of EMG was tested at 50–300 rpm. With the increase in rotating speed, the V_{OC} increases from 1.6 to 9.0 V (Fig. 4(d)), and the I_{SC} increases from 0.8 to 4.6 mA (Fig. 4(e)). The EMG load was tested at 200 rpm

(Fig. 4(f)). With the rise of external load resistance, the voltage increases from 0.3 to 6.0 V, and the current decreases from 3.2 to 0.2 mA. The maximum load power is 5.3 mW with a load of 2 k Ω . In agricultural production, harsh environments such as rain and snow often cause changes in environmental humidity. The V_{OC} and I_{SC} of EMG do not change with relative humidity change, displaying a stable output performance in harsh environments (Figs. 4(g) and 4(h)). The stability of EMG was tested at 50 rpm, and its V_{OC} is retained about 99.3% after 30,000 cycles (Fig. S6 in the ESM). As shown in Fig. 4(i), when TENG, EMG, and SMS-TEHG are used to charge the capacitor of 10 μ F, the voltage rise curve of TENG imparts good linearity. The upper voltage limit of TENG is higher than that of EMG, but the charging speed is slower than EMG, which is attributed to the different peak voltages of TENG and EMG at the same rotational speed. The voltage profile of SMS-TEHG is similar to that of EMG before the capacitor voltage rises to 5.6 V, and EMG is the main contributor at this stage. After the capacitor voltage exceeds 5.6 V, TENG is the main contributor. In short, when the wind speed is low, TENG can ensure that the capacitor can reach the voltage required by the appliance, and the contribution of EMG is less. When the wind speed increases in the environment, the EMG can make the capacitor reach the predetermined voltage faster.

2.4 Application in intelligent greenhouse

Sensors and control systems are essential for real-time monitoring of crop production, and the distributed power supply of sensors is a challenge. Figure 5(a) shows the applications of SMS-TEHG in intelligent greenhouse. A wind-driven SMS-TEHG is installed around the greenhouse to collect wind energy and convert it into electric power. The first application is to use SMS-TEHG to light 640 light-emitting diodes (LEDs) for nighttime light supplementation of crops in greenhouse (Fig. 5(b) and video ESM1). Figure S7 in the ESM illustrates the SMS-TEHG night light circuit diagram. EMG connects 320 LEDs in parallel, while

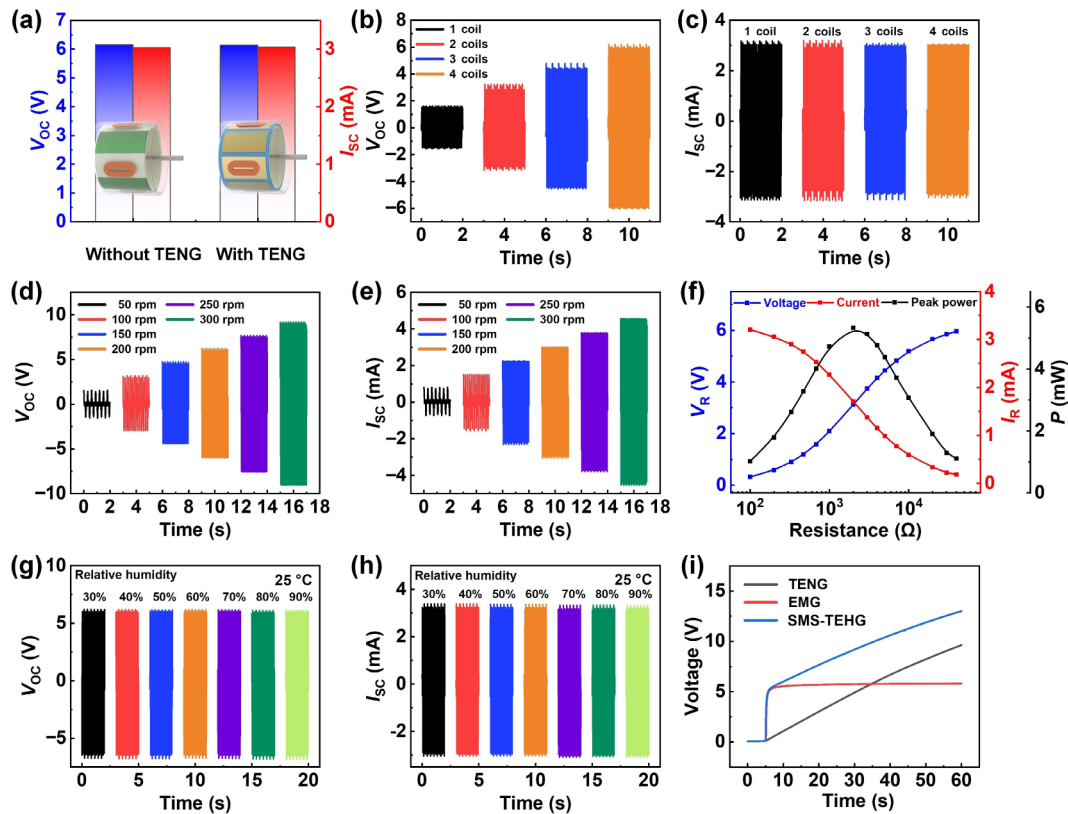


Figure 4 Electric output characteristics of EMG. (a) V_{OC} and I_{SC} with and without TENG. (b) V_{OC} and (c) I_{SC} of the electrode in different coil numbers. (d) and (e) Output performance at different speeds. (f) Output performance at different loads. The dependence of (g) V_{OC} and (h) I_{SC} of the EMG on the relative humidity from 30% to 90%. (i) The capacitor is charged by TENG, EMG, and SMS-TEHG at 200 rpm.

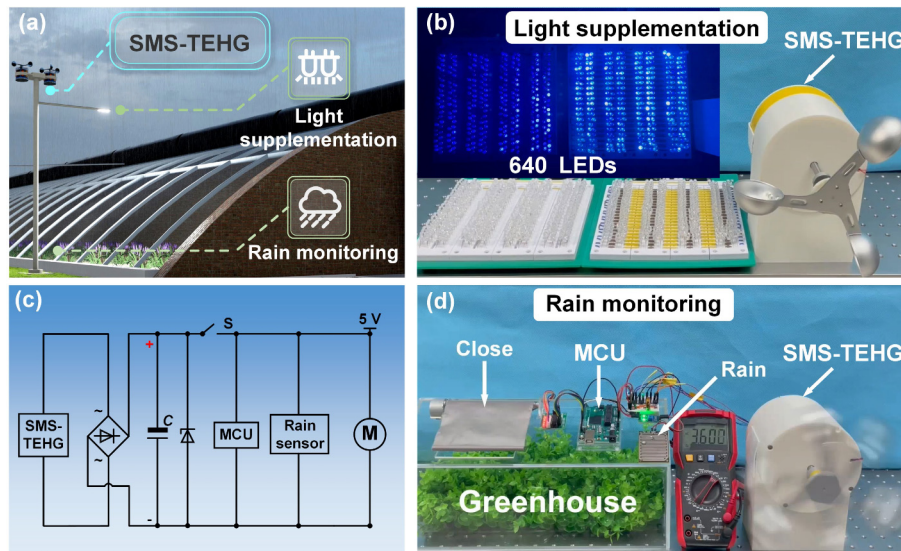


Figure 5 Applications of the SMS-TEHG in intelligent greenhouse. (a) The concept of SMS-TEHG in the greenhouse. (b) Light supplementation demonstration. (c) Circuit of a self-powered rain monitoring system. (d) Rain monitoring and control system.

TENG connects the remaining 320 LEDs in series. Figure 5(c) illustrates the rain sensing circuit. The electric signal of SMS-TEHG is converted from AC to direct current (DC) through the rectifier bridge, and charged to a 5 F supercapacitor. When the switch is closed, the capacitor supplies power to the microcontroller unit (MCU, Arduino), and the MCU begins to work. When the rain sensor is induced by rain, Arduino receives a signal to the motor to control the motor to drive the window closed. After the rain stops, MCU controls the motor to open the window. Then, a self-powered rain monitoring system is developed (Fig. 5(d) and video ESM2).

As shown in Fig. 6(a), a wireless temperature and humidity sensing system based on the SMS-TEHG power supply is

constructed by combining a temperature and humidity sensor, a central node, a cellular network, and mobile phone applications. The wireless temperature and humidity sensing system can be installed near the smart greenhouse to realize temperature and humidity monitoring (Fig. 6(b)). SMS-TEHG continuously collects wind energy and stores electric energy in a 0.1 F capacitor used as a temporary energy storage unit (Fig. 6(c)). SMS-TEHG supplies power to the commercial temperature and humidity sensor node with the ZigBee transmission function, which is set to send data to the central node once at an interval of 5 s. The central node sends the temperature and humidity information to the mobile phone through the cellular network. The temperature and humidity information is recorded and saved on the mobile phone.

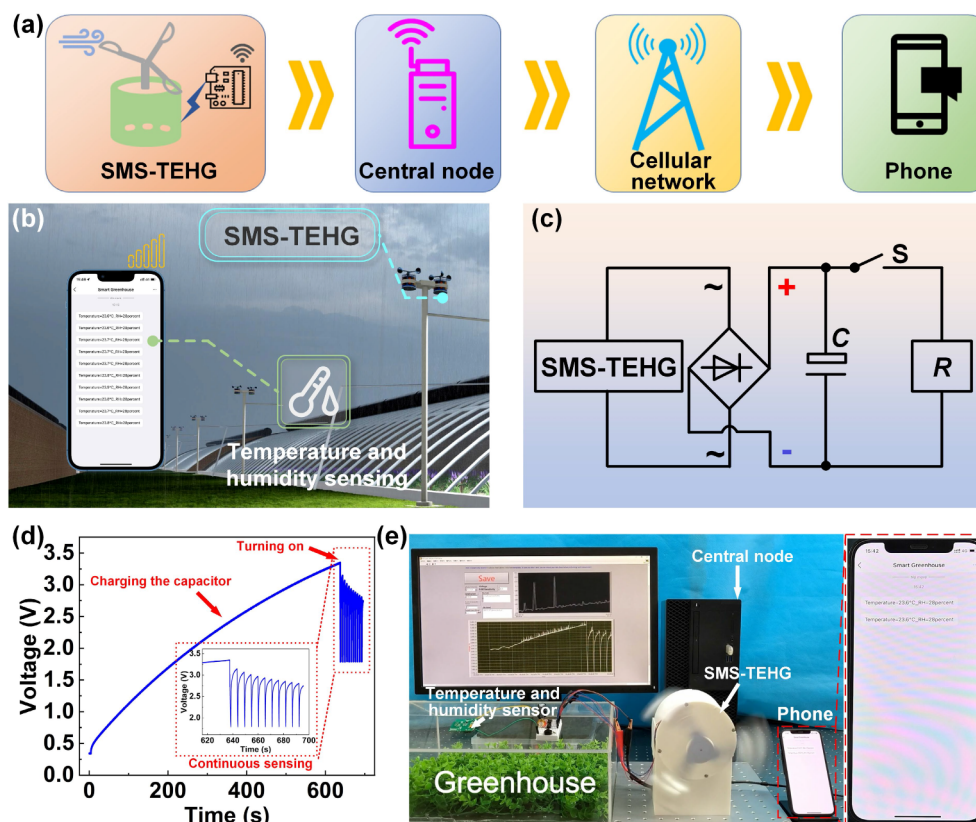


Figure 6 Demonstration of wireless temperature and humidity sensing powered by wind-driven SMS-TEHG. (a) Workflow diagram of self-powered wireless sensing. (b) Wireless temperature and humidity sensing powered by SMS-TEHG in the intelligent greenhouse. (c) Circuit diagram of wireless temperature and humidity sensing. (d) The capacitor voltage curve of the wireless temperature and humidity sensing system in operation. (e) Demonstration of wireless temperature and humidity sensing.

Figure 6(d) shows the capacitance voltage curve of the sensor node when it works. The demonstration system is shown in Fig. 6(e) and video ESM3. Unattended wireless monitoring is realized and the power supply difficulty is reduced.

3 Conclusions

In summary, a single-material-substrated triboelectric-electromagnetic hybrid generator (SMS-TEHG) based on flexible magnets is proposed for harvesting wind energy in smart agriculture. Flexible magnets serve as the electropositive triboelectric material for the TENG part and the magnetic material for the EMG part in SMS-TEHG, which combine the two parts and then simplify the structure of TEHG without affecting the output performance. The V_{OC} of TENG and EMG are 187.2 and 9.0 V at 300 rpm, respectively. SMS-TEHG has a peak power of 6.1 mW at 200 rpm. After 30,000 cycles of stability testing, the V_{OC} values of TENG and EMG retain about 95.6% and 99.3%, respectively. Moreover, self-powered applications powered by SMS-TEHG for intelligent greenhouses are successfully demonstrated, such as lighting 640 LEDs for crop light supplementation, rain monitoring and wireless temperature and humidity sensing. This paper provides a promising strategy for simplifying TEHG structure and developing a self-powered multifunctional intelligent greenhouse.

4 Experimental section

4.1 Fabrication of the SMS-TEHG

SMS-TEHG is made up of two components: EMG and TENG. 3D printing was used to construct the shafts, rotors, and stators of the EMG and TENG. The electrode was 0.08 mm thick. Double-sided

tape secured the magnets and coils to the rotor and stator. The flex magnet was 2 mm thick, and the coil had 2,200 turns. Figure S8 in the ESM illustrates the manufacturing process of coil. The PTFE film on several of the stator electrodes of TENG was 0.13 mm thick, and the flexible magnet was 36 mm × 80 mm. The surface topography of the flexible magnets was photographed by a light microscope (Leica DMI 3000B, Wetzlar, Germany).

4.2 Electrical measurement

The SMS-TEHG was driven by a servomotor (BSM001000000A, Mitsubishi, Korea) to measure various rotational speeds. A programmed electrometer evaluated the output performance of SMS-TEHG, including V_{OC} and I_{SC} (6514, Keithley, USA). The performance of SMS-TEHG at various relative humidity levels was assessed in a temperature and humidity-controlled test chamber (Y-HF-960L, Yuhang Zhida, China). The Arduino received the rain sensor signal and controlled the motor. The photographs of the components are shown in Fig. S9 in the ESM.

Acknowledgments

The authors are grateful for the support from the National Key Research & Development Project from the Minister of Science and Technology (Nos. 2021YFA1201601 and 2021YFA1201604), and the Beijing Natural Science Foundation (No. 3222023).

Electronic Supplementary Material: Supplementary material (additional figures and movies, including the flow chart for manufacturing the SMS-TEHG, electromagnetic simulation, the performance test of TENG charging to the capacitor, output performance of TENG at different rotating speeds, output performance of the EMG between the coil and the flexible magnet with and without TENG, stability test of EMG, light

supplementation circuit diagram, shape the coil using a mold, and photograph of components (lighting up 640 LEDs for light supplementation, and demonstration for rain monitoring, wireless temperature and humidity sensing powered by SMS-TEHG)) is available in the online version of this article at <https://doi.org/10.1007/s12274-022-4922-1>.

References

- [1] Basso, B.; Antle, J. Digital agriculture to design sustainable agricultural systems. *Nat. Sustain.* **2020**, *3*, 254–256.
- [2] Yin, H. Y.; Cao, Y. T.; Marelli, B.; Zeng, X. Q.; Mason, A. J.; Cao, C. Y. Soil sensors and plant wearables for smart and precision agriculture. *Adv. Mater.* **2021**, *33*, 2007764.
- [3] Araújo, S. O.; Peres, R. S.; Barata, J.; Lidon, F.; Ramalho, J. C. Characterising the agriculture 4.0 landscape—Emerging trends, challenges and opportunities. *Agronomy* **2021**, *11*, 667.
- [4] Zhao, X.; Askari, H.; Chen, J. Nanogenerators for smart cities in the era of 5G and internet of things. *Joule* **2021**, *5*, 1391–1431.
- [5] Lan, L. Y.; Xiong, J. Q.; Gao, D. C.; Li, Y.; Chen, J.; Lv, J.; Ping, J. F.; Ying, Y. B.; Lee, P. S. Breathable nanogenerators for an on-plant self-powered sustainable agriculture system. *ACS Nano* **2021**, *15*, 5307–5315.
- [6] Giraldo, J. P.; Wu, H. H.; Newkirk, G. M.; Kruss, S. Nanobiotechnology approaches for engineering smart plant sensors. *Nat. Nanotechnol.* **2019**, *14*, 541–553.
- [7] Zhang, P.; Guo, Z. L.; Ullah, S.; Melagraki, G.; Afantitis, A.; Lynch, I. Nanotechnology and artificial intelligence to enable sustainable and precision agriculture. *Nat. Plants* **2021**, *7*, 864–876.
- [8] Fan, F. R.; Tian, Z. Q.; Wang, Z. L. Flexible triboelectric generator. *Nano Energy* **2012**, *1*, 328–334.
- [9] Wang, Z. L. Triboelectric nanogenerators as new energy technology and self-powered sensors—Principles, problems and perspectives. *Faraday Discuss.* **2014**, *176*, 447–458.
- [10] Zhang, C.; Tang, W.; Han, C. B.; Fan, F. R.; Wang, Z. L. Theoretical comparison, equivalent transformation, and conjunction operations of electromagnetic induction generator and triboelectric nanogenerator for harvesting mechanical energy. *Adv. Mater.* **2014**, *26*, 3580–3591.
- [11] Wang, Z. L. On Maxwell's displacement current for energy and sensors: The origin of nanogenerators. *Mater. Today* **2017**, *20*, 74–82.
- [12] Wang, Z. L.; Wang, A. C. On the origin of contact-electrification. *Mater. Today* **2019**, *30*, 34–51.
- [13] Wang, Z. L. Triboelectric nanogenerator (TENG)—Sparking an energy and sensor revolution. *Adv. Energy Mater.* **2020**, *10*, 2000137.
- [14] Yang, Z. B.; Zhou, S. X.; Zu, J.; Inman, D. High-performance piezoelectric energy harvesters and their applications. *Joule* **2018**, *2*, 642–697.
- [15] Wu, C. S.; Wang, A. C.; Ding, W. B.; Guo, H. Y.; Wang, Z. L. Triboelectric nanogenerator: A foundation of the energy for the new era. *Adv. Energy Mater.* **2019**, *9*, 1802906.
- [16] Liang, X.; Jiang, T.; Liu, G. X.; Feng, Y. W.; Zhang, C.; Wang, Z. L. Spherical triboelectric nanogenerator integrated with power management module for harvesting multidirectional water wave energy. *Energy Environ. Sci.* **2020**, *13*, 277–285.
- [17] Zhang, B. S.; Tang, Y. J.; Dai, R. R.; Wang, H. Y.; Sun, X. P.; Qin, C.; Pan, Z. F.; Liang, E. J.; Mao, Y. C. Breath-based human-machine interaction system using triboelectric nanogenerator. *Nano Energy* **2019**, *64*, 103953.
- [18] Zhang, N.; Qin, C.; Feng, T. X.; Li, J.; Yang, Z. R.; Sun, X. P.; Liang, E. J.; Mao, Y. C.; Wang, X. D. Non-contact cylindrical rotating triboelectric nanogenerator for harvesting kinetic energy from hydraulics. *Nano Res.* **2020**, *13*, 1903–1907.
- [19] Ning, C.; Tian, L.; Zhao, X. Y.; Xiang, S. X.; Tang, Y. J.; Liang, E. J.; Mao, Y. C. Washable textile-structured single-electrode triboelectric nanogenerator for self-powered wearable electronics. *J. Mater. Chem. A* **2018**, *6*, 19143–19150.
- [20] Xie, L. J.; Zhai, N. N.; Liu, Y. N.; Wen, Z.; Sun, X. H. Hybrid triboelectric nanogenerators: From energy complementation to integration. *Research* **2021**, *2021*, 9143762.
- [21] Wang, L. Y.; Wang, Y.; Wang, H.; Xu, G. Q.; Döring, A.; Daoud, W. A.; Xu, J. B.; Rogach, A. L.; Xi, Y.; Zi, Y. L. Carbon dot-based composite films for simultaneously harvesting raindrop energy and boosting solar energy conversion efficiency in hybrid cells. *ACS Nano* **2020**, *14*, 10359–10369.
- [22] Xu, L. Y.; Xu, L.; Luo, J. J.; Yan, Y.; Jia, B. E.; Yang, X. D.; Gao, Y. H.; Wang, Z. L. Hybrid all-in-one power source based on high-performance spherical triboelectric nanogenerators for harvesting environmental energy. *Adv. Energy Mater.* **2020**, *10*, 2001669.
- [23] Zhai, N. N.; Wen, Z.; Chen, X. P.; Wei, A. M.; Sha, M.; Fu, J. J.; Liu, Y. N.; Zhong, J.; Sun, X. H. Blue energy collection toward all-hours self-powered chemical energy conversion. *Adv. Energy Mater.* **2020**, *10*, 2001041.
- [24] Ye, C. Y.; Dong, K.; An, J.; Yi, J.; Peng, X.; Ning, C.; Wang, Z. L. A triboelectric–electromagnetic hybrid nanogenerator with broadband working range for wind energy harvesting and a self-powered wind speed sensor. *ACS Energy Lett.* **2021**, *6*, 1443–1452.
- [25] Zhang, B. S.; Zhang, S.; Li, W. B.; Gao, Q.; Zhao, D.; Wang, Z. L.; Cheng, T. H. Self-powered sensing for smart agriculture by electromagnetic–triboelectric hybrid generator. *ACS Nano* **2021**, *15*, 20278–20286.
- [26] Xu, S. H.; Fu, X. P.; Liu, G. X.; Tong, T.; Bu, T. Z.; Wang, Z. L.; Zhang, C. Comparison of applied torque and energy conversion efficiency between rotational triboelectric nanogenerator and electromagnetic generator. *iScience* **2021**, *24*, 102318.
- [27] Li, Z. J.; Saadatnia, Z.; Yang, Z. B.; Naguib, H. A hybrid piezoelectric–triboelectric generator for low-frequency and broadband energy harvesting. *Energy Convers. Manage.* **2018**, *174*, 188–197.
- [28] Wang, S. H.; Wang, Z. L.; Yang, Y. A one-structure-based hybridized nanogenerator for scavenging mechanical and thermal energies by triboelectric–piezoelectric–pyroelectric effects. *Adv. Mater.* **2016**, *28*, 2881–2887.
- [29] Kim, S. W.; Yang, U. J.; Lee, J. W.; Kim, F.; Kim, Y.; Lee, G.; Son, J. S.; Baik, J. M. Triboelectric charge-driven enhancement of the output voltage of bisbte-based thermoelectric generators. *ACS Energy Lett.* **2021**, *6*, 1095–1103.
- [30] Lee, D.; Kim, I.; Kim, D. Hybrid tribo-thermoelectric generator for effectively harvesting thermal energy activated by the shape memory alloy. *Nano Energy* **2021**, *82*, 105696.
- [31] Zhang, T. T.; Wen, Z.; Liu, Y. N.; Zhang, Z. Y.; Xie, Y. L.; Sun, X. H. Hybridized nanogenerators for multifunctional self-powered sensing: Principles, prototypes, and perspectives. *iScience* **2020**, *23*, 101813.
- [32] Mu, J. L.; Zou, J.; Song, J. S.; He, J.; Hou, X. J.; Yu, J. B.; Han, X. T.; Feng, C. P.; He, H. C.; Chou, X. J. Hybrid enhancement effect of structural and material properties of the triboelectric generator on its performance in integrated energy harvester. *Energy Convers. Manage.* **2022**, *254*, 115151.
- [33] Fang, Y.; Tang, T. Y.; Li, Y. F.; Hou, C.; Wen, F.; Yang, Z.; Chen, T.; Sun, L. N.; Liu, H. C.; Lee, C. A high-performance triboelectric–electromagnetic hybrid wind energy harvester based on rotational tapered rollers aiming at outdoor IoT applications. *iScience* **2021**, *24*, 102300.
- [34] Liu, L.; Shi, Q. F.; Lee, C. A hybridized electromagnetic–triboelectric nanogenerator designed for scavenging biomechanical energy in human balance control. *Nano Res.* **2021**, *14*, 4227–4235.
- [35] Shao, H. Y.; Cheng, P.; Chen, R. X.; Xie, L. J.; Sun, N.; Shen, Q. Q.; Chen, X. P.; Zhu, Q. Q.; Zhang, Y.; Liu, Y. N. et al. Triboelectric–electromagnetic hybrid generator for harvesting blue energy. *Nano-Micro Lett.* **2018**, *10*, 54.
- [36] Fan, X. M.; He, J.; Mu, J. L.; Qian, J. C.; Zhang, N.; Yang, C. J.; Hou, X. J.; Geng, W. P.; Wang, X. D.; Chou, X. J. Triboelectric–electromagnetic hybrid nanogenerator driven by wind for self-powered wireless transmission in internet of things and self-powered wind speed sensor. *Nano Energy* **2020**, *68*, 104319.